

# Efficient Energy Stable Schemes with Spectral Discretization in Space for Anisotropic Cahn-Hilliard Systems

Feng Chen and Jie Shen\*

*Department of Mathematics, Purdue University, West Lafayette, IN 47907-1957, USA.*

Received 10 November 2011; Accepted (in revised version) 11 May 2012

Available online 8 October 2012

---

**Abstract.** We develop in this paper efficient and robust numerical methods for solving anisotropic Cahn-Hilliard systems. We construct energy stable schemes for the time discretization of the highly nonlinear anisotropic Cahn-Hilliard systems by using a stabilization technique. At each time step, these schemes lead to a sequence of linear coupled elliptic equations with constant coefficients that can be efficiently solved by using a spectral-Galerkin method. We present numerical results that are consistent with earlier work on this topic, and also carry out various simulations, such as the linear bi-Laplacian regularization and the nonlinear Willmore regularization, to demonstrate the efficiency and robustness of the new schemes.

**AMS subject classifications:** 65N35, 65M12, 35K55

**Key words:** Spectral-Galerkin, phase-field, anisotropic, Cahn-Hilliard, stabilization, coupled elliptic equations.

---

## 1 Introduction

The phase-field method has been frequently used in the study of the dynamics of heterogeneous materials, such as crystal growth, phase separations in binary mixtures, and multi-phase fluid flows. Its ubiquitous advantage over the sharp-interface approach is that there is no need to track the interface explicitly. Usual phase-field approaches often lead to a second-order Allen-Cahn equations [1] or a fourth-order Cahn-Hilliard equation [3]. It is usually more challenging to solve the Cahn-Hilliard equation than the Allen-Cahn equation due to its high-order nature and its stiffness caused by small parameters in the physical system.

We consider in this paper a classical problem in materials science, namely, determining the equilibrium shape of a solid crystal in its own liquid matrix. When anisotropy

---

\*Corresponding author. *Email addresses:* feng\_chen\_1@brown.edu (F. Chen), shen@math.purdue.edu (J. Shen)

of the micro-mechanical system is sufficiently strong, the surface energy function,  $f(\phi)$ , may become too large or singular on certain orientations. Thus, these orientations may be missing in the equilibrium shape (or Wulff shape) in order to achieve a well-defined energy for the system. Consequently, the equilibrium interface will not be a smooth curve, but present facets and corners with slope discontinuities (cf. [17]). Fundamentally, the gradient energy density loses its convexity (see a proof in the Appendix of [20]) when the so-called 'surface stiffness' changes its sign (cf. [10] for the sharp interface approach on the same topic). In this case, the corresponding Cahn-Hilliard equation is intrinsically of a backward parabolic type. Thus it is an ill-posed problem and requires regularizations. The linear bi-Laplacian regularization and the nonlinear Willmore regularization (cf. [6, 7, 11]) will be considered in this paper. While the former is easier to deal with numerically, its asymptotic results does not match the correct physics. The latter is more physically consistent, with sharp corners of the Wulff shape replaced by rounded corners while major parts of edges remains unchanged, but its free energy is also much more complicated. Both regularizations lead to a sixth-order Cahn-Hilliard type equations which present significant challenges for developing efficient and accurate numerical schemes. There are two main difficulties: (i) the presence of a small parameter  $\epsilon$ , representing the interfacial width, which makes the (time continuous) discretized system very stiff; and (ii) the high-order spatial derivatives, which make the spatially discretized system very difficult to solve.

In [8], the authors used a second-order central difference discretization in space for solving the anisotropic Cahn-Hilliard equation. A convexification technique was employed so that the regularization was not needed. However, it used an explicit time discretization, resulting in severe time step restrictions. In the recent work [18, 20], the authors solved the regularized anisotropic Cahn-Hilliard system with an adaptive nonlinear multigrid finite difference method.

We propose to solve the regularized anisotropic Cahn-Hilliard systems with a stabilized time discretization that allows large time steps and a spectral discretization in space. Unlike in [18, 20], our numerical schemes do not lead to a nonlinear system at each time step, instead, only a system of three coupled linear elliptic equations with constant coefficients that can be efficiently solved by a suitable spectral method.

The paper is organized as follows: in Section 2, we describe the governing PDE system for the anisotropic crystal growth. The main idea of the paper is given in Section 3, where we propose our time discretizations and spectral methods for the system. Numerical tests and simulations are given in Section 4. We conclude with a few remarks in the last section.

## 2 Phase-field models for anisotropic systems

Let  $\Omega \subset \mathbb{R}^d$  ( $d=2,3$ ), and  $\phi(\mathbf{x})$  be an order parameter that takes the values  $\pm 1$  in the two phases with a smooth transitional layer of thickness  $\epsilon$ . We consider the following free

energy density of Ginzburg-Landau type,

$$\mathcal{F}(\phi) = \frac{\gamma(\mathbf{n})}{\epsilon} \left( f(\phi) + \frac{\epsilon^2}{2} |\nabla\phi|^2 \right), \tag{2.1}$$

where  $\gamma(\mathbf{n})$  is a function describing the anisotropic property and  $\mathbf{n}$  is the interface normal defined as

$$\mathbf{n} = (n_1, n_2)^T = \frac{\nabla\phi}{|\nabla\phi|}, \tag{2.2}$$

and the energy density  $f(\phi)$  takes the usual form

$$f(\phi) = \frac{1}{4} (\phi^2 - 1)^2. \tag{2.3}$$

Then, the surface energy of the system is given by

$$\mathcal{E}(\phi) = \int_{\Omega} \mathcal{F}(\phi) d\Omega. \tag{2.4}$$

The difference between an isotropic system and an anisotropic one is reflected in different choices of  $\gamma(\mathbf{n})$  in (2.1). When  $\gamma(\mathbf{n}) \equiv 1$ , we have an isotropic system, namely, the free energy has no preference in orientations. In this case, the  $H^{-1}$ -gradient flow of (2.4) leads to the usual isotropic Cahn-Hilliard equation. In the anisotropic case,  $\gamma(\mathbf{n})$  depends on  $\mathbf{n}$  in a nontrivial manner. We consider in this paper the fourfold symmetric anisotropic function,

$$\gamma(\mathbf{n}) = 1 + \alpha \cos(4\theta) = 1 + \alpha \left( 4 \sum_{i=1}^d n_i^4 - 3 \right), \tag{2.5}$$

where  $\theta$  denotes the orientation angle of the interfacial normal to the interface. The non-negative parameter  $\alpha$  in (2.5) describes the intensity of anisotropy. When  $\alpha=0$ , the system is reduced to the isotropic case. As  $\alpha$  increases, the system becomes more anisotropic. It is indicated in [18,20] that a sufficient big  $\alpha$  would produce a strongly anisotropic system, i.e., the underline Cahn-Hilliard equation is ill-posed. In order to regularize the original problem, an extra term,  $\mathcal{G}$ , is added to (2.4) to penalize infinite curvatures in the resulting corners. Consequently, the total system energy becomes

$$\mathcal{E}(\phi) = \int_{\Omega} \left( \mathcal{F} + \frac{\beta}{2} \mathcal{G} \right) d\Omega, \tag{2.6}$$

where  $\beta$  is a small regularization parameter. We consider two kinds of regularizations, namely, two different forms of  $\mathcal{G}$ .

The first one is the linear regularization based on the bi-Laplacian of the phase variable,

$$\mathcal{G}_L(\phi) = \frac{1}{\epsilon^3} (\epsilon^2 \Delta\phi)^2 = \epsilon |\Delta\phi|^2. \tag{2.7}$$

By taking the  $H^{-1}$ -gradient flow on (2.6), we derive the anisotropic Cahn-Hilliard system with the linear regularization:

$$\begin{cases} \phi_t = \frac{1}{\epsilon} \Delta \mu, \\ \mu = \frac{\gamma(\mathbf{n})}{\epsilon} f'(\phi) - \epsilon \nabla \cdot \mathbf{m} - \beta \Delta \omega, \\ \omega = -\epsilon \Delta \phi. \end{cases} \quad (2.8)$$

In the above, the chemical potential  $\mu$  is the variational derivative of  $\mathcal{E}$ , and the vector field  $\mathbf{m}$  is given by

$$\mathbf{m} = \gamma(\mathbf{n}) \nabla \phi + \mathbb{P} \nabla_n \gamma(\mathbf{n}) \left( \frac{f}{\epsilon^2 |\nabla \phi|} + \frac{1}{2} |\nabla \phi| \right) \quad \text{with } \mathbb{P} = \mathbb{I} - \mathbf{n} \otimes \mathbf{n}. \quad (2.9)$$

In the isotropic case, i.e., with  $\gamma(\mathbf{n}) = 1$  in the above, we obtain the isotropic Cahn-Hilliard system with linear regularization

$$\begin{cases} \phi_t = \frac{1}{\epsilon} \Delta \mu, \\ \mu = \frac{\delta \mathcal{E}}{\delta \phi} = \frac{1}{\epsilon} f(\phi) + \omega - \beta \Delta \omega, \\ \omega = -\epsilon \Delta \phi. \end{cases} \quad (2.10)$$

The second choice, which is more effective as an approximation to the consistent sharp-interface model as pointed out in [18], is the following nonlinear Willmore regularization,

$$\mathcal{G}_N(\phi) = \omega^2, \quad (2.11)$$

where  $\omega$  is variational derivative of the isotropic part of  $\mathcal{F}$ , i.e.,

$$\omega = \frac{1}{\epsilon} f'(\phi) - \epsilon \Delta \phi. \quad (2.12)$$

By taking the  $H^{-1}$ -gradient flow on (2.6), we derive the strongly anisotropic Cahn-Hilliard system with the Willmore regularization:

$$\begin{cases} \phi_t = \frac{1}{\epsilon} \nabla \cdot [M(\phi) \nabla \mu], \\ \mu = \frac{\delta \mathcal{E}}{\delta \phi} = \frac{\gamma(\mathbf{n})}{\epsilon} f'(\phi) - \epsilon \nabla \cdot \mathbf{m} + \frac{\beta}{\epsilon^2} \omega f''(\phi) - \beta \Delta \omega, \\ \omega = \frac{1}{\epsilon} f'(\phi) - \epsilon \Delta \phi, \end{cases} \quad (2.13)$$

where  $m$  is defined in (2.9). For simplicity, we focus on the bulk diffusion case and set the mobility function  $M(\phi)$  to be 1. The system (2.13) is supplemented with either the homogeneous Neumann boundary condition,

$$\frac{\partial \phi}{\partial \mathbf{n}} \Big|_{\partial \Omega} = \frac{\partial \mu}{\partial \mathbf{n}} \Big|_{\partial \Omega} = \frac{\partial \omega}{\partial \mathbf{n}} \Big|_{\partial \Omega} = 0, \quad (2.14)$$

or the  $2\pi$ -periodic boundary condition for  $\phi$ ,  $\mu$ , and  $\omega$ .

By taking the inner product of the first equation of (2.13) with  $\mu$ , the second equation with  $\phi_t$ , and subtracting two resulted equations, one derives that the system (2.13) admits the following energy law:

$$\frac{d}{dt} \mathcal{E}(\phi) = -\frac{1}{\epsilon} \|\nabla \mu\|^2. \quad (2.15)$$

Note that the expression for  $m$  may cause significant difficulties in numerical simulation due to the presence of the term  $\frac{1}{\epsilon} \frac{f}{|\nabla \phi|}$ . Therefore, we follow [18] to use the following approximate form

$$m \approx \gamma(\mathbf{n}) \nabla \phi + |\nabla \phi| \mathbb{P} \nabla_{\mathbf{n}} \gamma(\mathbf{n}), \quad (2.16)$$

which is obtained by using the fact that near the interface we have (cf. [18])

$$f(\phi) \sim (\epsilon^2/2) |\nabla \phi|^2. \quad (2.17)$$

However, with this approximation, the systems (2.8) and (2.13) no longer satisfy the energy law (2.15), but it has been numerically proven in [18] that the energy is non-increasing.

### 3 Numerical schemes

The nonlinear Cahn-Hilliard systems derived in the above all have sixth-order spatial derivatives and develop interfaces with thickness of order  $\epsilon$ . It is a great challenge to develop efficient and stable numerical schemes for them.

The difficulty associated with the small interfacial width in a phase-field approach is usually dealt with either the convex splitting method (cf., for instance, [9, 19]) or the stabilized method (cf., for instance, [15, 21]).

We shall construct efficient numerical schemes for the three nonlinear Cahn-Hilliard systems (2.10), (2.8), (2.13), and in the first case, prove rigorously that the proposed scheme is energy stable. For the second and third cases, since their corresponding spatial continuous cases do not satisfy the energy law (2.15), it is not possible to prove the numerical schemes are energy stable.

We shall follow three general principles in designing time discretization schemes for these systems: (i) all the diffusion terms should be treated implicitly, a necessary condition for the scheme to be stable; (ii) all nonlinear terms are treated explicitly to avoid solving nonlinear equations at each time step; (iii) adding a stabilizing term to avoid the severe time step constraint due to the explicit treatment of nonlinear terms.

### 3.1 Isotropic case with the linear regularization

We consider first the isotropic Cahn-Hilliard system (2.10). The full understanding of this simpler problem is important because it provides guidance for designing better schemes in the other two cases. We propose the following stabilized first-order scheme:

$$\begin{cases} \frac{\phi^{n+1} - \phi^n}{\delta t} = \frac{1}{\epsilon} \Delta \mu^{n+1}, \\ \mu^{n+1} = \frac{1}{\epsilon} f'(\phi^n) + \omega^{n+1} - \beta \Delta \omega^{n+1} + \frac{s}{\epsilon} (\phi^{n+1} - \phi^n), \\ \omega^{n+1} = -\epsilon \Delta \phi^{n+1}, \end{cases} \quad (3.1)$$

where  $s$  is a stabilization constant.

We note that the additional stabilizing term  $s(\phi^{n+1} - \phi^n)/\epsilon$  introduces a consistency error of order  $\mathcal{O}(s\frac{\delta t}{\epsilon})$  that is of the same order as treating the term  $\frac{1}{\epsilon} f(\phi)$  explicitly. We refer to [15, 22] for remarks on similar schemes for the Allen-Cahn and Cahn-Hilliard equations.

In order to describe the stability, we define the discrete energy  $\mathcal{E}^n$  for (3.1) as

$$\mathcal{E}^n \triangleq \mathcal{E}(\phi^n) = \int_{\Omega} (\mathcal{F}(\phi^n) + \frac{\beta}{2} \mathcal{G}_L(\phi^n)) d\Omega = \frac{1}{\epsilon} (f(\phi^n), 1) + \frac{\epsilon}{2} \|\nabla \phi^n\|^2 + \frac{\beta\epsilon}{2} \|\Delta \phi^n\|^2. \quad (3.2)$$

**Theorem 3.1.** *The solution of (3.1) obeys the following discrete energy law:*

$$\frac{1}{\delta t} (\mathcal{E}^{n+1} - \mathcal{E}^n) \leq -\frac{1}{\epsilon} \|\nabla \mu^{n+1}\|^2, \quad n = 0, 1, \dots, \quad (3.3)$$

if

$$\delta t \leq \frac{4\epsilon^4}{L^2} \quad \text{when } s=0, \quad \text{or } s \geq \frac{L}{2}, \quad (3.4)$$

where  $L \triangleq \max_{\phi \in \mathbb{R}} |f''(\phi)|$ .

*Proof.* Taking the inner product of the first equation of (3.1) with  $\delta t \mu^{n+1}$ , we obtain

$$(\phi^{n+1} - \phi^n, \mu^{n+1}) = -\frac{\delta t}{\epsilon} \|\nabla \mu^{n+1}\|^2. \quad (3.5)$$

Taking the inner product of the second equation of (3.1) with  $\phi^{n+1} - \phi^n$ , we derive

$$(\phi^{n+1} - \phi^n, \mu^{n+1}) = I + II, \quad (3.6)$$

where

$$I = \frac{1}{\epsilon} (f'(\phi^n), \phi^{n+1} - \phi^n), \quad (3.7a)$$

$$II = \left( \omega^{n+1} - \beta \Delta \omega^{n+1} + \frac{s}{\epsilon} (\phi^{n+1} - \phi^n), \phi^{n+1} - \phi^n \right). \quad (3.7b)$$

Expanding  $f(\phi^{n+1})$  at  $\phi^n$  with Taylor formula, we have

$$f(\phi^{n+1}) = f(\phi^n) + f'(\phi^n)(\phi^{n+1} - \phi^n) + \frac{1}{2}f''(\xi^n)(\phi^{n+1} - \phi^n)^2, \tag{3.8}$$

where  $\xi^n$  is between  $\phi^{n+1}$  and  $\phi^n$ . Hence we can rewrite  $I$  as

$$I = \frac{1}{\epsilon} \left( f(\phi^{n+1}) - f(\phi^n), 1 \right) - \frac{1}{2\epsilon} \left( f''(\xi^n)(\phi^{n+1} - \phi^n), (\phi^{n+1} - \phi^n) \right). \tag{3.9}$$

Next we split  $II$  into three parts,

$$II = II_a + II_b + II_c, \tag{3.10}$$

where

$$II_a = (\omega^{n+1}, \phi^{n+1} - \phi^n) = \epsilon(\nabla\phi^{n+1}, \nabla(\phi^{n+1} - \phi^n)), \tag{3.11a}$$

$$II_b = -\beta(\Delta\omega^{n+1}, \phi^{n+1} - \phi^n) = \epsilon\beta(\Delta\phi^{n+1}, \Delta(\phi^{n+1} - \phi^n)), \tag{3.11b}$$

$$II_c = \frac{s}{\epsilon}(\phi^{n+1} - \phi^n, \phi^{n+1} - \phi^n) = \frac{s}{\epsilon}\|\phi^{n+1} - \phi^n\|^2. \tag{3.11c}$$

Using the algebraic identity,

$$2(a, a-b) = a^2 - b^2 + (a-b)^2, \tag{3.12}$$

we can rewrite  $II_a$  and  $II_b$  as

$$II_a = \frac{\epsilon}{2} \left( \|\nabla\phi^{n+1}\|^2 - \|\nabla\phi^n\|^2 + \|\nabla(\phi^{n+1} - \phi^n)\|^2 \right), \tag{3.13a}$$

$$II_b = \frac{\epsilon\beta}{2} \left( \|\Delta\phi^{n+1}\|^2 - \|\Delta\phi^n\|^2 + \|\Delta(\phi^{n+1} - \phi^n)\|^2 \right). \tag{3.13b}$$

Combining (3.5), (3.6), (3.9), (3.11) and (3.13), we obtain

$$\mathcal{E}^{n+1} - \mathcal{E}^n + \frac{\epsilon}{2}\|\nabla(\phi^{n+1} - \phi^n)\|^2 + \frac{\delta t}{\epsilon}\|\nabla\mu^{n+1}\|^2 + \frac{1}{\epsilon} \left( s - \frac{1}{2}f''(\xi^n) \right) \|\phi^{n+1} - \phi^n\|^2 \leq 0. \tag{3.14}$$

**Case  $s=0$ :** We take the inner product of (3.1) with  $\epsilon\sqrt{\delta t}(\phi^{n+1} - \phi^n)$ , obtaining

$$\begin{aligned} \frac{\epsilon}{\sqrt{\delta t}}\|\phi^{n+1} - \phi^n\|^2 &= -\sqrt{\delta t}(\nabla\mu^{n+1}, \nabla(\phi^{n+1} - \phi^n)) \\ &\leq \frac{\delta t}{2\epsilon}\|\nabla\mu^{n+1}\|^2 + \frac{\epsilon}{2}\|\nabla(\phi^{n+1} - \phi^n)\|^2. \end{aligned} \tag{3.15}$$

Summing up the last two relations, we get

$$\mathcal{E}^{n+1} - \mathcal{E}^n + \left( \frac{\epsilon}{\sqrt{\delta t}} - \frac{1}{2\epsilon}f''(\xi^n) \right) \|\phi^{n+1} - \phi^n\|^2 \leq 0. \tag{3.16}$$

Hence, we have  $\mathcal{E}^{n+1} - \mathcal{E}^n \leq 0$  if  $\delta t \leq \frac{4\epsilon^4}{L^2}$ .

**Case  $s > 0$ :** We obtain immediately from (3.14) that  $\mathcal{E}^{n+1} - \mathcal{E}^n \leq 0$  under the assumption  $s \geq \frac{1}{2}$ .  $\square$

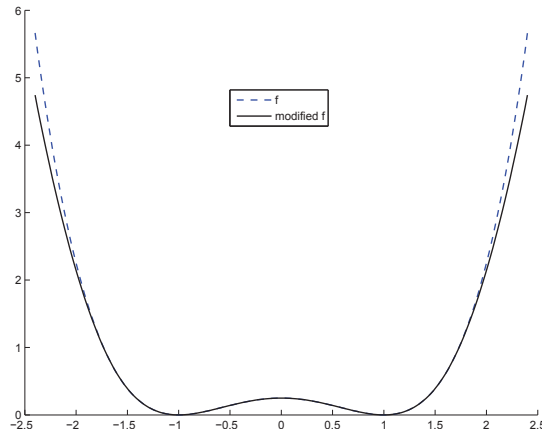


Figure 1:  $f$  and  $\tilde{f}$  with  $K=1.6$ .

**Remark 3.1.** Note that for the usual double-well potential  $f(\phi)$ ,  $L = \infty$ . However, it is shown in [2] that the solution of a usual Cahn-Hilliard system will not be affected if we replace the quartic growth of  $f(\phi)$  at infinities by quadratic growth, e.g.,

$$\tilde{f} = \begin{cases} \frac{3K^2-1}{2}\phi^2 - 2K^3\phi + \frac{1}{4}(3K^4+1), & \phi > K, \\ \frac{1}{4}(\phi^2-1)^2, & \phi \in [-K, K], \\ \frac{3K^2-1}{2}\phi^2 + 2K^3\phi + \frac{1}{4}(3M^4+1), & \phi < -K, \end{cases} \quad (3.17)$$

with a sufficiently large positive number  $K$ . Hence, we can expect that replacing  $f$  by  $\tilde{f}$  will not affect the solution of system (2.10). For notational simplicity, we still denote  $\tilde{f}$  by  $f$ .

**Remark 3.2.** One can easily construct a second order stabilized scheme, for example:

$$\begin{cases} \frac{3\phi^{n+1} - 4\phi^n + \phi^{n-1}}{2\delta t} = \frac{1}{\epsilon} \Delta \mu^{n+1}, \\ \mu^{n+1} = \frac{1}{\epsilon} (2f'(\phi^n) - f'(\phi^{n-1})) + \omega^{n+1} - \beta \Delta \omega^{n+1} + \frac{s}{\epsilon} (\phi^{n+1} - 2\phi^n + \phi^n), \\ \omega^{n+1} = -\epsilon \Delta \phi^{n+1}. \end{cases} \quad (3.18)$$

However, this scheme is no longer unconditionally stable, but our numerical experiments indicate that the allowable time step can be orders of magnitude larger than the usual semi-implicit scheme (cf. also [15]). Note that one can construct second-order accurate numerical schemes to gradient system with an unconditional energy stability by using the convex splitting technique (cf. [9, 14, 19]). However, these schemes lead to a nonlinear system at each time step.

**Remark 3.3.** The proof of Theorem 3.1 is based on an energy argument with a weak formulation of (3.1). Therefore, the proof can be carried over to the fully discrete case as long as the spatial discretization is based on a consistent weak formulation.

### 3.2 Anisotropic case with the linear regularization

We now consider the anisotropic system with the linear bi-Laplacian regularization (2.8).

We propose the following first order stabilized scheme:

$$\begin{cases} \frac{\phi^{n+1} - \phi^n}{\delta t} = \frac{1}{\epsilon} \Delta \mu^{n+1}, \\ \mu^{n+1} = \frac{1}{\epsilon} [\gamma(\mathbf{n}^n) f'(\phi^n) - \epsilon^2 \nabla \cdot \mathbf{m}^n] - \beta \Delta \omega^{n+1} + \frac{s}{\epsilon} (\phi^{n+1} - \phi^n) + \tilde{s} (\omega^{n+1} - \omega^n), \\ \omega^{n+1} = -\epsilon \Delta \phi^{n+1}. \end{cases} \quad (3.19)$$

Different from the scheme (3.1), there are two stabilizing terms in the second equation of the above scheme. As in (3.1), the first stabilizing term,  $s(\phi^{n+1} - \phi^n)/\epsilon$ , is introduced to balance the explicit treatment of  $\frac{1}{\epsilon} \gamma(\mathbf{n}) f'(\phi)$ , while the second stabilizing term,  $\tilde{s}(\omega^{n+1} - \omega^n)$ , is introduced to balance the explicit treatment of  $\epsilon \nabla \cdot \mathbf{m}$ . In fact, when we take the inner product of the second equation in (3.19) with  $\phi^{n+1} - \phi^n$ , we have  $\tilde{s}(\omega^{n+1} - \omega^n, \phi^{n+1} - \phi^n) = \tilde{s} \epsilon \|\nabla(\phi^{n+1} - \phi^n)\|^2$ . Note that the term needs to be stabilized is

$$\epsilon(\nabla \cdot \mathbf{m}^n, \phi^{n+1} - \phi^n) = -\epsilon(\mathbf{m}^n, \nabla(\phi^{n+1} - \phi^n)). \quad (3.20)$$

Taking into account the approximate form of  $\mathbf{m}$  given in (2.16), we see that this term can be controlled by the stabilizing term for  $\tilde{s}$  sufficiently large (but independent of  $\epsilon$ ). Indeed, while it is not possible to prove an analog of Theorem 3.1 due to the fact that the system (2.8) uses (2.16), but our numerical results indicate that for suitably large  $\tilde{s}$  and  $s$ , the scheme (3.21) is energy dissipative for arbitrary  $\delta t$ .

### 3.3 Anisotropic case with the Willmore regularization

We now construct a stabilized scheme for (2.13). Unlike in (2.8), there is a nonlinear term in the expression for  $\omega$  that needs to be stabilized. Hence, we consider the following stabilized scheme:

$$\begin{cases} \frac{\phi^{n+1} - \phi^n}{\delta t} = \frac{1}{\epsilon} \Delta \mu^{n+1}; \\ \mu^{n+1} = \frac{1}{\epsilon} [\gamma(\mathbf{n}^n) f'(\phi^n) - \epsilon^2 \nabla \cdot \mathbf{m}^n] + \frac{\beta}{\epsilon^2} [\tilde{s}(\omega^{n+1} - \tilde{\omega}^n) + f''(\phi^n) \tilde{\omega}^n] - \beta \Delta \omega^{n+1}, \\ \text{where } \tilde{\omega}^n = \frac{1}{\epsilon} f'(\phi^n) - \epsilon \Delta \phi^n; \\ \omega^{n+1} = \frac{1}{\epsilon} [s(\phi^{n+1} - \phi^n) + f'(\phi^n) - \epsilon^2 \Delta \phi^{n+1}]. \end{cases} \quad (3.21)$$

We now explain why we use  $\tilde{\omega}^n$ , instead of  $\omega^n$ , in the expression for  $\mu^{n+1}$ . We derive from the last relation in the above scheme that

$$\omega^{n+1} - \omega^n = \frac{s}{\epsilon}(\phi^{n+1} - 2\phi^n + \phi^{n-1}) + \frac{1}{\epsilon}(f'(\phi^n) - f'(\phi^{n-1})) - \epsilon(\Delta\phi^{n+1} - \Delta\phi^n). \quad (3.22)$$

Hence, if we use, as the stabilization term,  $\tilde{s}(\omega^{n+1} - \omega^n)$ , instead of  $\tilde{s}(\omega^{n+1} - \tilde{\omega}^n)$ , in the expression for  $\mu^{n+1}$ , it will not provide enough stabilization due to the the second-order term  $(\phi^{n+1} - 2\phi^n + \phi^{n-1})$ . Indeed, our numerical results show that the associated scheme is not energy dissipative. On the other hand, we have

$$\omega^{n+1} - \tilde{\omega}^n = \frac{s}{\epsilon}(\phi^{n+1} - \phi^n) - \epsilon(\Delta\phi^{n+1} - \Delta\phi^n), \quad (3.23)$$

so the inner product of this term with  $\phi^{n+1} - \phi^n$  provides sufficient stabilization.

As for the scheme (3.19), it is not possible to prove an analog of Theorem 3.1, but our numerical results indicate that for suitably large  $\tilde{s}$  and  $s$ , the scheme (3.21) is indeed energy dissipative, hence stable, for arbitrary  $\delta t$ .

### 3.4 Spatial discretization

We recall that all the nonlinear terms in our schemes are explicitly treated so that we have a linear system to solve at each time step. More precisely, for schemes (3.1), (3.19), or (3.21), a system of three coupled elliptic equations needs to be solved at each time step. Taking (3.21) as an example, it can be rearranged as

$$\begin{cases} \frac{\epsilon}{\delta t}\phi^{n+1} - \Delta\mu^{n+1} = \frac{\epsilon}{\delta t}\phi^n, \\ \frac{1}{\beta}\mu^{n+1} - \frac{\tilde{s}\omega^{n+1}}{\epsilon^2} + \Delta\omega^{n+1} = \frac{1}{\beta\epsilon}(\gamma(\mathbf{n}^n)f'(\phi^n) - \epsilon^2\nabla \cdot \mathbf{m}^n) + \frac{1}{\epsilon^2}f''(\phi^n)\tilde{\omega}^n - \frac{\tilde{s}\tilde{\omega}^n}{\epsilon^2}, \\ \frac{1}{\epsilon}\omega^{n+1} - \frac{s}{\epsilon^2}\phi^{n+1} + \Delta\phi^{n+1} = -\frac{s}{\epsilon^2}\phi^n + \frac{1}{\epsilon^2}f'(\phi^n). \end{cases} \quad (3.24)$$

Hence, at each time step, we only need to solve the following prototype system of coupled elliptic equations,

$$\begin{cases} \alpha u + \beta v + \gamma w - \eta \Delta w = f, \\ \tilde{\alpha} u + \tilde{\beta} v + \tilde{\gamma} w - \tilde{\eta} \Delta v = g, \\ \tilde{\tilde{\alpha}} u + \tilde{\tilde{\beta}} v + \tilde{\tilde{\gamma}} w - \tilde{\tilde{\eta}} \Delta u = h, \end{cases} \quad (3.25)$$

where  $\{u, v, w\}$  are unknown solutions,  $\{f, g, h\}$  are given right hand side functions, and all the coefficients are constants. We shall use spectral methods to solve this system of equations along with suitable boundary conditions.

If the system (3.25) is supplemented with the boundary conditions (2.14), we shall use a new spectral-Galerkin method for solving systems of coupled elliptic equations

recently developed in [5]. For the readers' convenience, we provide below a very brief description of the method in the two-dimensional case.

Let us denote

$$X_N = \{v \in P_N : \partial_x v|_{\pm 1} = 0; \mathbb{X}_N = X_N \times X_N\}. \tag{3.26}$$

Setting  $\phi_k(x) = L_k(x) - \frac{k(k+1)}{(k+2)(k+3)}L_{k+2}(x)$ , it is easy to check that  $X_N = \text{span}\{\phi_k : k = 0, 1, \dots, q = N-2\}$  (cf. [12]). Expanding the approximate solutions to  $(u, v, w)$  as

$$(u_N, v_N, w_N) = \sum_{k=0}^q \sum_{j=0}^q (\tilde{u}_{kj}, \tilde{v}_{kj}, \tilde{w}_{kj}) \phi_k(x) \phi_j(y), \tag{3.27}$$

and setting

$$U_{kj} = \tilde{u}_{kj}, \quad V_{kj} = \tilde{v}_{kj}, \quad W_{kj} = \tilde{w}_{kj}, \quad M_{kj} = (\phi_j, \phi_k), \quad S_{kj} = (\phi'_j, \phi'_k), \tag{3.28a}$$

$$F_{kj} = (I_N f, \phi_k(x) \phi_j(y)), \quad G_{kj} = (I_N g, \phi_k(x) \phi_j(y)), \quad H_{kj} = (I_N h, \phi_k(x) \phi_j(y)), \tag{3.28b}$$

the Legendre-Galerkin method to (3.25) is equivalent to the following system of matrix equations [12, 13]:

$$\begin{cases} \alpha MUM + \beta MVM + \gamma MWM + \eta(SUM + MUS) = F, \\ \tilde{\alpha} MUM + \tilde{\beta} MVM + \tilde{\gamma} MWM + \tilde{\eta}(SUM + MUS) = G, \\ \tilde{\tilde{\alpha}} MUM + \tilde{\tilde{\beta}} MVM + \tilde{\tilde{\gamma}} MWM + \tilde{\tilde{\eta}}(SUM + MUS) = H. \end{cases} \tag{3.29}$$

The above system can be solved efficiently by a matrix diagonalization method recently developed in [5]. More precisely, the computational complexity for solving the system of three coupled equations (3.25) is essentially three times of the cost for solving one Poisson type equation by the efficient Legendre-Galerkin method [12]. Therefore, this method is very efficient and spectrally accurate.

For the case of periodic boundary conditions, the system (3.25) can be solved very efficiently by a straightforward Fourier-Galerkin method (cf., for instance, [4, 13]). Namely, let  $\tilde{f}_k, \tilde{g}_k$  and  $\tilde{h}_k$  be the  $\mathbf{k}$  Fourier-coefficient of the given functions  $f, g, h$ , and  $\tilde{u}_k, \tilde{v}_k$  and  $\tilde{w}_k$  be the  $\mathbf{k}$  Fourier-coefficient of the unknown functions  $u, v, w$ . Then, the system (3.25) is reduced to a sequence of  $3 \times 3$  algebraic system: for each  $\mathbf{k} \in \mathbb{N}^d$ , find  $\tilde{u}_k, \tilde{v}_k$  and  $\tilde{w}_k$  from

$$\begin{cases} \alpha \tilde{u}_k + \beta \tilde{v}_k + \gamma \tilde{w}_k + \eta |\mathbf{k}|^2 \tilde{w}_k = \tilde{f}_k, \\ \tilde{\alpha} \tilde{u}_k + \tilde{\beta} \tilde{v}_k + \tilde{\gamma} \tilde{w}_k + \tilde{\eta} |\mathbf{k}|^2 \tilde{v}_k = \tilde{g}_k, \\ \tilde{\tilde{\alpha}} \tilde{u}_k + \tilde{\tilde{\beta}} \tilde{v}_k + \tilde{\tilde{\gamma}} \tilde{w}_k + \tilde{\tilde{\eta}} |\mathbf{k}|^2 \tilde{u}_k = \tilde{h}_k, \end{cases} \tag{3.30}$$

which can be inverted directly.

Note that the explicit nonlinear terms in all cases are computed using the usual pseudo-spectral approach.

## 4 Numerical simulations and discussion

We present in this section various numerical examples to show the robustness and effectiveness of our numerical schemes, and to validate the phase field model for the strongly anisotropic system. In Subsection 4.1, we show time evolutions of phase interfaces for the three different models using the corresponding schemes presented in Section 3. In Subsection 4.2, we simulate the roughing process for a sinusoidal curve, and study quantitatively the anisotropy phenomenon of the Wulff shape. The impact of regularizations is studied in Subsection 4.3 where we compare the linear regularization and Willmore regularization by using the Legendre-Galerkin method. In addition, the asymptotic convergence as  $\beta \rightarrow 0$  of Willmore regularizations is observed numerically.

In all simulations, we assume  $\Omega = (-1, 1)^2$  with the homogeneous Neumann boundary conditions in (2.14), and use the Legendre-Galerkin method with  $129 \times 129$  modes described in the last section. We have used a time step  $\delta = 10^{-3}$  in all simulations. This choice is not made by stability requirement, as our schemes are all unconditionally stable, rather, it is made by the accuracy requirement.

### 4.1 Effectiveness tests and time evolutions

For each of the examples show below using the (3.1), (3.19), or (3.21), we have numerically verified that these schemes with  $s = \tilde{s} = 2$  are unconditionally stable with any  $\delta t$ . Hence, the choice of time step  $\delta t$  is only dictated by the accuracy requirement, not the stability.

#### 4.1.1 Isotropic case with the linear regularization

As the first example, consider the isotropic Cahn-Hilliard system with the linear regularization, (2.10), and the corresponding scheme (3.1). We use the following parameters,

$$\delta t = 10^{-3}, \quad T = 0.7, \quad \epsilon = 0.02, \quad \beta = 10^{-4}, \quad s = 2, \quad (4.1)$$

where  $\delta t$  is time step size,  $T$  the terminating time,  $\epsilon$  proportional to the interfacial width,  $\beta$  the regularization parameter, and  $s$  the stabilization parameter. We choose the initial condition as

$$\phi_0(x, y) = \sum_{i=1}^3 \tanh \frac{\sqrt{(x-x_i)^2 + (y-y_i)^2} - r_i}{\epsilon} - 2, \quad (4.2)$$

where  $\{x_i, y_i\}_{i=1}^3$  and  $\{r_i\}_{i=1}^3$  are circle centers and radii. The time evolution of the zero-isocontours of  $\phi$  are shown in the top part of Fig. 2, while the energy evolution is shown in the bottom of Fig. 2.

We observe clearly the coarsening effect of the Cahn-Hilliard system, and the conservation of volume fraction. We also observe that the energy is non-increasing, as proved in Theorem 3.1, and achieves its equilibrium at around  $t = 0.65$  (650 time steps). Note in particular that the energy undergoes a rapid decrease when the first and second small circles are absorbed into the large circle.

We note that the scheme (3.1) (with  $s = 0$ ) would blow up quickly for all  $\delta t > 10^{-7}$ .

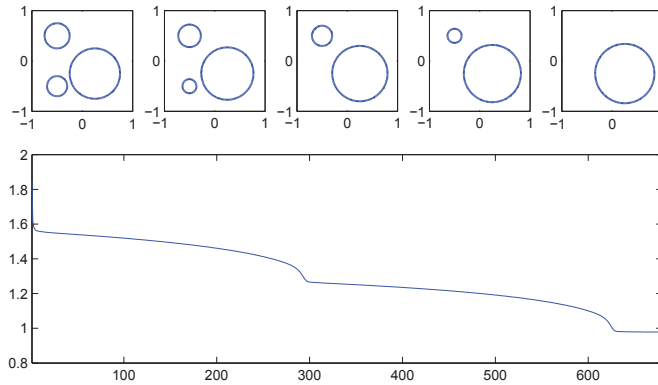


Figure 2: The time evolution by the scheme of (3.1) with parameters in (4.1). Top: zero-isocontours of the phase variable at  $t_i=iT/4$ , for  $i=0,1,2,3,4$ . Bottom: the energy evolution in term of the number of time steps.

#### 4.1.2 Anisotropic case with the linear regularization

We now consider the anisotropic Cahn-Hilliard system with the linear regularization, (2.7), using the scheme (3.19) with the initial condition

$$\phi_0(x,y) = \tanh\left(\frac{\sqrt{x^2+y^2}-r}{\epsilon}\right), \tag{4.3}$$

and the parameters

$$\delta t = 10^{-3}, \quad T = 0.22, \quad \epsilon = 0.02, \quad \beta = 6 \times 10^{-4}, \quad \alpha = 0.3, \quad s = 2, \quad \tilde{s} = 2, \tag{4.4}$$

where  $\alpha$  is the anisotropy parameter,  $r$  the radius of the initial circle, both  $s$  and  $\tilde{s}$  stabilization parameters, and other parameters have the same meaning as in (4.1).

The top row in Fig. 3 shows how an isotropic interface with full orientations evolves to an anisotropic one with missing orientations at four corners. The energy (the bottom row in Fig. 3) is also non-decreasing with the given choices of  $s$  and  $\tilde{s}$ . We note that, without these stabilization terms, the scheme (3.19) (with  $s = \tilde{s} = 0$ ) would blow up quickly for all  $\delta t > 10^{-7}$ .

#### 4.1.3 Anisotropic case with the Willmore regularization

We now consider (2.13) using the scheme (3.21) with the parameters

$$\delta t = 10^{-3}, \quad T = 0.15, \quad \epsilon = 0.02, \quad \beta = 5 \times 10^{-4}, \quad \alpha = 0.3, \quad s = 2, \quad \tilde{s} = 2. \tag{4.5}$$

In the first example, we use the initial condition given by (4.3) with  $r = 0.5$ . The left plot in Fig. 4 shows how the interface evolves from a circle to a square of Wulff shape. The right plot in Fig. 4 shows the energy evolution in time. These results are in very good agreement with those presented in [20].

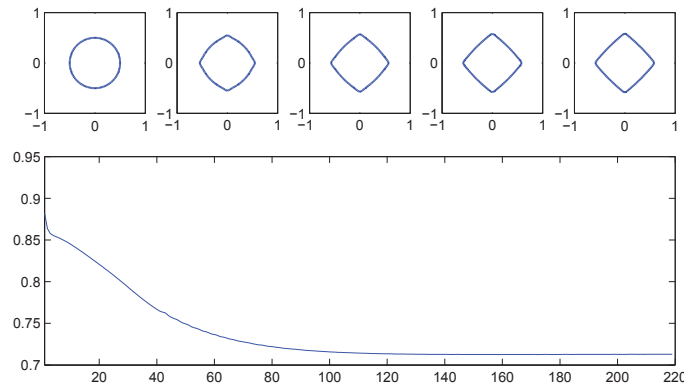


Figure 3: The time evolution of the scheme of (3.19). Top: zero-isocontours of the phase variable at  $t_i = iT/4$ , for  $i=0,1,2,3,4$ . Bottom: the energy evolution in term of the number of time steps.

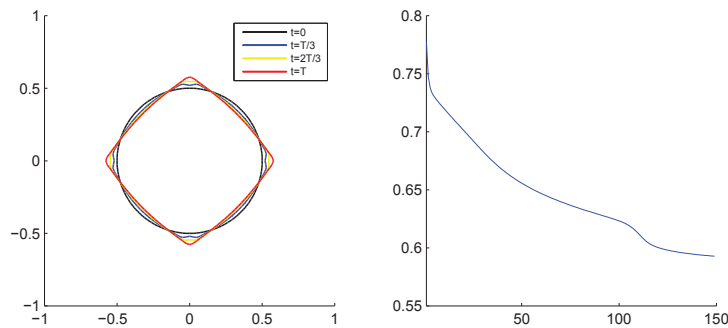


Figure 4: (Color online) The first example in Subsection 4.1.3. Left: zero-isocontours of the phase variable at  $t_i = iT/3$ , for  $i=0,1,2,3$ . Right: the energy evolution in term of the number of time steps.

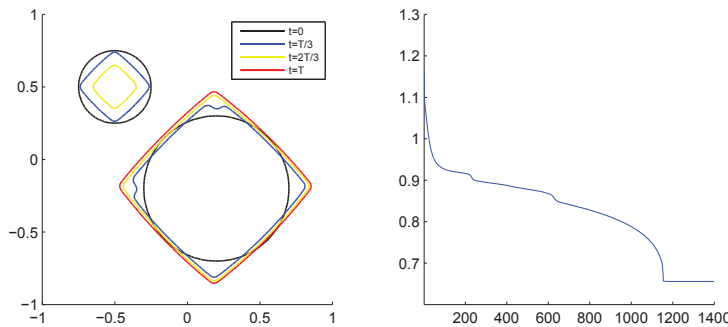


Figure 5: (Color online) The second example in Subsection 4.1.3. Left: zero-isocontours of the phase variable at  $t_i = iT/3$ , for  $i=0,1,2,3$ . Right: the energy evolution in term of the number of time steps.

In the second example, we start with the initial condition given in Fig. 5, and use the same parameters as in (4.5) except a larger  $T$  to reach the equilibrium.

We observe two simultaneous effects in this evolution (cf. Fig. 5): the anisotropy effect and the coarsening effect.

The left of Fig. 5 shows that the anisotropy process takes place first, followed by the coarsening process during which the two squares merge into one. The energy evolution in the right of Fig. 5 shows that the merging completes at around  $T = 1.18$  (1180 time steps).

Once again, the scheme (3.21) without the stabilization terms (i.e.,  $s = \tilde{s} = 0$ ) blows up quickly for all  $\delta t > 10^{-8}$ .

## 4.2 Anisotropy and missing orientations

We study below the anisotropic effect by using two examples: (i) the roughing process of a smooth curve; and (ii) missing orientations in the Wulff shape with different  $\alpha$  values. We demonstrate that our numerical simulations capture various anisotropy phenomena effectively.

### 4.2.1 Strong anisotropy of a rough curve

An interesting example is the evolution of a sinusoidal interface to a facet interface with corners and kinks [8, 20] (see the evolution in Fig. 6). We use the scheme (3.21) with the following initial condition,

$$\phi_0(x, y) = \tanh\left(\frac{y - \frac{r(x)}{2}}{2\sqrt{2}\epsilon}\right), \tag{4.6}$$

where

$$r(x) = 0.4\cos(\pi x) + 0.4\cos(3\pi x) + 0.2\cos(5\pi x) + 0.06\cos(7\pi x). \tag{4.7}$$

The following parameters are used,

$$\delta t = 10^{-3}, \quad T = 0.9, \quad \epsilon = 0.03, \quad \beta = 0.004, \quad \alpha = 0.3, \quad s = 2, \quad \tilde{s} = 2. \tag{4.8}$$

We observe in Fig. 6 that the equilibrium shape is finally dominated by the largest initial mode, which is  $0.4\cos(\pi x)$ .

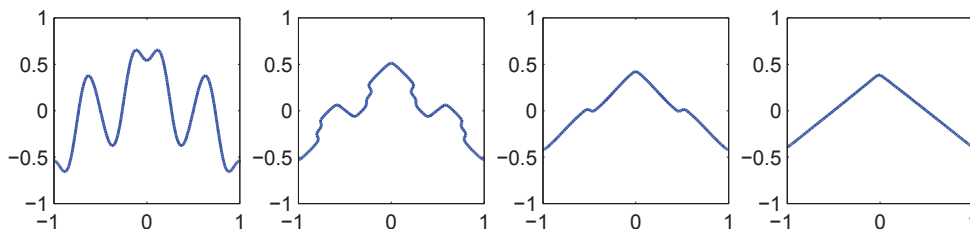


Figure 6: The evolution of the interface from a sinusoidal curve to a facet curve.

#### 4.2.2 Missing orientations of the Wulff shape

We simulate below the missing orientations of the benchmark problem, i.e., the evolution of a circle to a square shown in the first example of Subsection 4.1.3. We will show that as  $\alpha$  becomes sufficiently large, the solution will reach an anisotropic equilibrium.

We use the scheme (3.21) with the parameters in (4.5) except different  $\alpha$ 's are used.

The equilibrium shapes with different  $\alpha$  values are shown in the top panel of Fig. 7, while the polar plots of the interface normal angles,  $\theta$ , as a function of the coordinate angle,  $\nu$ , are given on the bottom panel. We observe that when  $\alpha$  is relatively small, e.g.  $\alpha = 0.1$  (the top left plot in Fig. 7), the anisotropy is not strong enough, so there are no evident missing orientations. When the anisotropy is not sufficiently strong,  $\theta$  changes continuously from 0 to  $2\pi$  as a function of  $\nu$ . As  $\alpha$  becomes larger, the gradient energy function is non-convex and the equation becomes anisotropic and four missing orientations appear in the four corners (the top middle and top right plots in Fig. 7).

We observe that there are clear discrepancies for the values of  $\gamma$  at  $\theta = 0, \pi/2, \pi, 3\pi/2$ . However, it is not completely discontinuous because of the regularizations. The four sharp corners were rounded and there are still points in between the angles near corners in the polar plots. Fundamentally, the regularization changes the original ill-posed problem into a different but well-posed one.

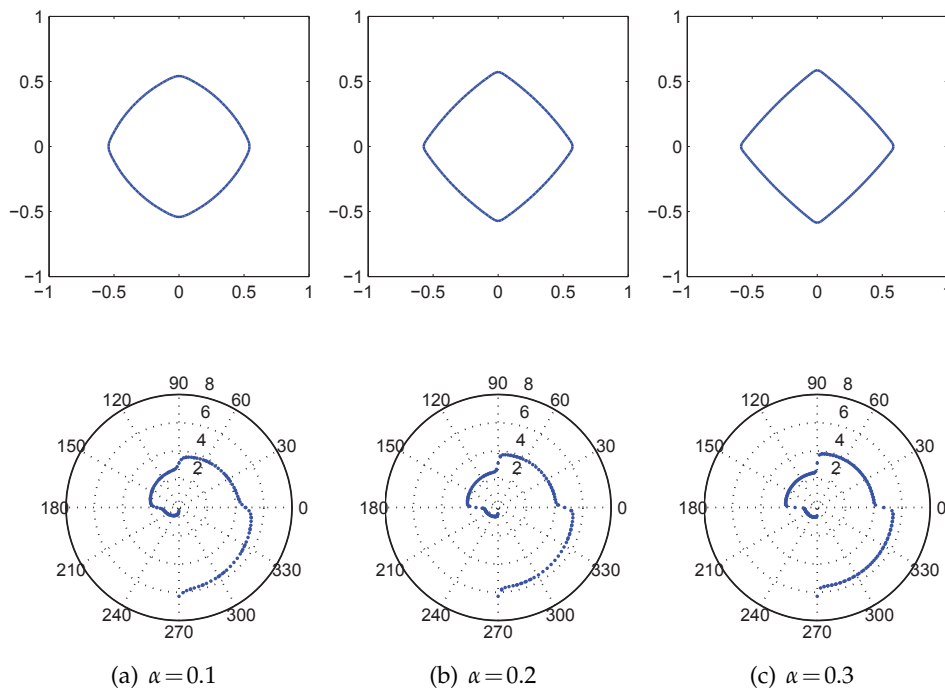


Figure 7: Top: equilibrium shapes with different  $\alpha$  values. Bottom: orientation angles in the polar coordinate.

### 4.3 Comparison between Linear and Willmore regularizations

In the last subsection of numerical simulations, we show that the nonlinear Willmore regularization yields more consistent asymptotic convergence towards the non-regularized anisotropic Cahn-Hilliard equation than the linear regularization does, by comparing our numerical results with the asymptotic analytic solution in [16]. We use the two schemes (3.19) and (3.21) with the same initial condition of a circular interface with radius  $r=0.625$ .

For the linear regularization, the numerical solution reaches its equilibrium at around  $T = 1$ . Comparing the regularized solution and the asymptotic solution (the left plot in Fig. 8), one observes apparent mismatches on both the edges and corner parts, even with very small  $\beta$  values (e.g.  $\beta = 10^{-4}$ ). The situation is different in case of the Willmore regularization. The right plot in Fig. 8 contains equilibrium interfaces of Wulff shapes with four different  $\beta$  values. All of their edges and corners match the asymptotic result more closely than in the linear regularization. The plots with four different  $\beta$  values are indistinguishable in Fig. 8, but one can see their differences in the zoomed Fig. 9. This observation is also in agreement with the theoretical and numerical results in [18].

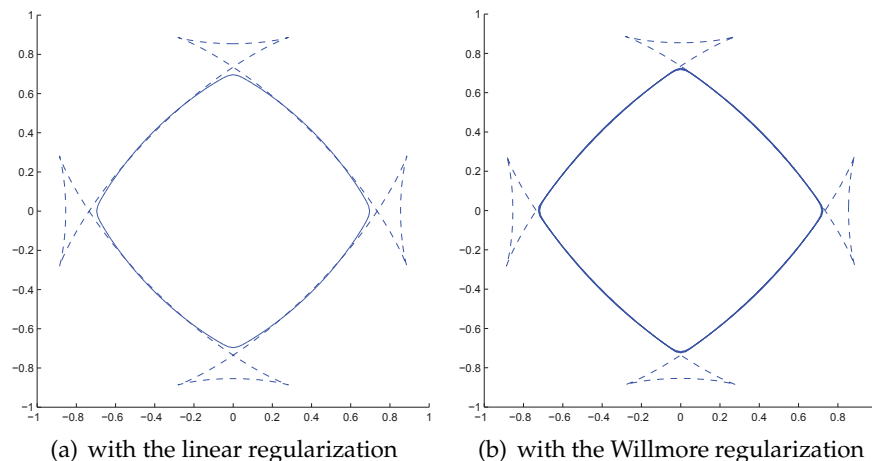


Figure 8: (Color online) The comparison between the linear regularization and the Willmore regularization.

A closer look at Fig. 9 indicates that the numerical solution with anisotropic regularization converges to the asymptotic solution as  $\beta$  approaches to zero. We also observe from the energy evolution presented in Fig. 10 that different values of  $\beta$  may lead to different energy dissipating patterns. In particular, the case with  $\beta = 4 \times 10^{-4}$  corresponds to the two-hill-one-valley structure evolution discussed in Subsection 4.1.3.

## 5 Conclusions

We developed in this paper efficient and robust numerical methods for solving anisotropic Cahn-Hilliard systems that are sixth-order nonlinear parabolic type equations. These sys-

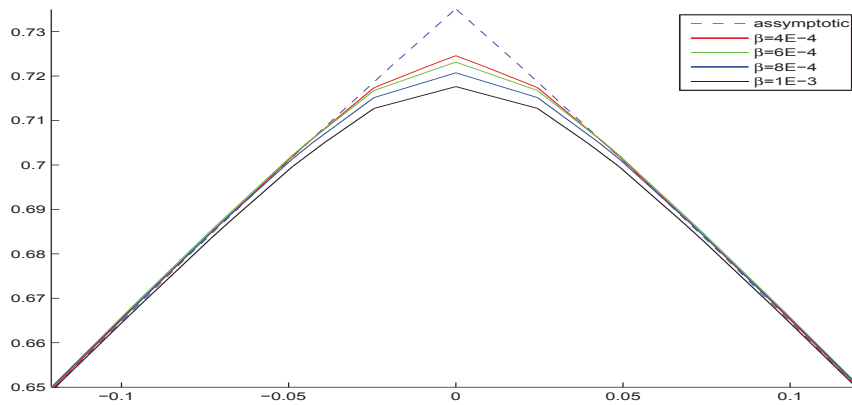


Figure 9: (Color online) The top corner of the right plot in Fig. 8: enlarged.

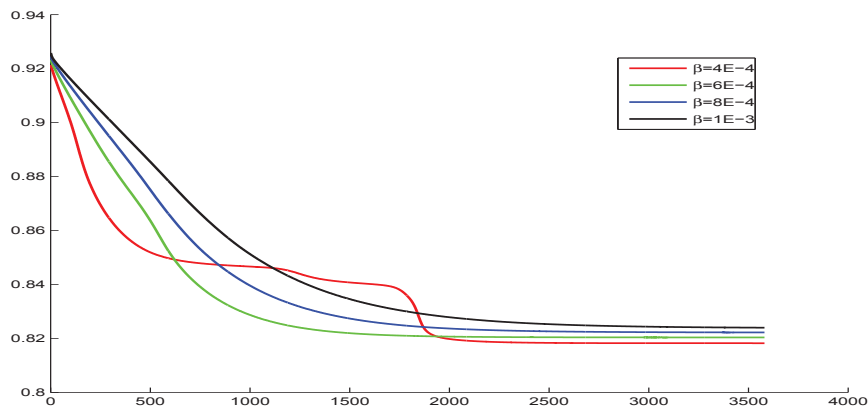


Figure 10: (Color online) The energy evolutions with four different  $\beta$  used in Fig. 9.

tems are notoriously difficult to solve numerically due to stiffness caused by the small parameter  $\epsilon$ , and the high-order spatial derivatives.

We constructed stabilized time discretization schemes for the highly nonlinear anisotropic Cahn-Hilliard systems. We showed rigorously in the simplest case and verified numerically in the other cases, that the scheme is unconditionally energy stable. At each time step, these schemes lead to a sequence of linear coupled elliptic equations with constant coefficients that can be efficiently solved by using a spectral-Galerkin method. Thus, our numerical schemes are very efficient for solving the anisotropic Cahn-Hilliard systems.

We presented ample numerical results that are consistent with earlier work, indicating that our stabilized schemes are capable of capturing correct evolution dynamics and equilibrium states. We also carried out various simulations, such as the linear bi-Laplacian regularization and the nonlinear Willmore regularization, to demonstrate the efficiency and robustness of the new schemes.

## Acknowledgments

This work is partially supported by NSF grant DMS-0915066 and AFOSR grant FA9550-11-1-0328.

## References

- [1] S. M. Allen and J. W. Cahn. A microscopic theory for antiphase boundary motion and its application to antiphase domain coarsening. *Acta Metall. Mater.*, 27:1085–1095, 1979.
- [2] L. A. Caffarelli and N. E. Muler. An  $L^\infty$  bound for solutions of the Cahn-Hilliard equation. *Archive for Rational Mechanics and Analysis*, 133(2):129–144, 1995.
- [3] J. W. Cahn and J. E. Hilliard. Free energy of a nonuniform system, I: Interfacial free energy. *J. Chem. Phys.*, 28:258, 1958.
- [4] C. Canuto, M. Y. Hussaini, A. Quarteroni, and T. A. Zang. *Spectral methods. Scientific Computation.* Springer-Verlag, Berlin, 2006. Fundamentals in single domains.
- [5] F. Chen and J. Shen. Efficient spectral-Galerkin methods for systems of coupled second-order equations and their applications. *J. Comput. Phys.*, 231(15):5016–5028, June 2012.
- [6] E. De Giorgi. Some remarks on  $\Gamma$ -convergence and least squares method. In *Composite media and homogenization theory (Trieste, 1990)*, volume 5 of *Progr. Nonlinear Differential Equations Appl.*, pages 135–142. Birkhäuser Boston, Boston, MA, 1991.
- [7] Q. Du, C. Liu, R. Ryham, and X. Wang. A phase field formulation of the Willmore problem. *Nonlinearity*, 18(3):1249–1267, 2005.
- [8] J. J. Eggleston, G. B. McFadden, and P. W. Voorhees. A phase-field model for highly anisotropic interfacial energy. *Phys. D*, 150(1-2):91–103, 2001.
- [9] D. J. Eyre. Unconditionally gradient stable time marching the Cahn-Hilliard equation. In *Computational and mathematical models of microstructural evolution (San Francisco, CA, 1998)*, volume 529 of *Mater. Res. Soc. Sympos. Proc.*, pages 39–46. MRS, Warrendale, PA, 1998.
- [10] M. E. Gurtin. *Thermomechanics of Evolving Phase Boundaries in the Plane.* Oxford University Press, USA, June 1993.
- [11] A. Ratz and A. Voigt. Higher order regularization of anisotropic geometric evolution equations in three dimensions. *Journal of Computational and Theoretical Nanoscience*, 3:560–564, August 2006.
- [12] J. Shen. Efficient spectral-Galerkin method I: direct solvers of second- and fourth-order equations using Legendre polynomials. *SIAM J. Sci. Comput.*, 15(6):1489–1505, 1994.
- [13] J. Shen, T. Tang, and L.-L. Wang. *Spectral Methods: Algorithms, Analysis and Applications*, volume 41 of *Springer Series in Computational Mathematics.* Springer, 2011.
- [14] J. Shen, C. Wang, X. Wang, and S. M. Wise. Second-order convex splitting schemes for gradient flows with Ehrlich-Schwoebel type energy: Application to thin film epitaxy. *SIAM Journal on Numerical Analysis*, 50(1):105–125, 2012.
- [15] J. Shen and X. Yang. Numerical approximations of Allen-Cahn and Cahn-Hilliard equations. *Discrete and Continuous Dynamical Systems*, 28(4):1669–1691, June 2010.
- [16] B. J. Spencer. Asymptotic solutions for the equilibrium crystal shape with small corner energy regularization. *Physical Review E*, 69(1):011603, 2004.
- [17] J. E. Taylor and J. W. Cahn. Diffuse interfaces with sharp corners and facets: phase field models with strongly anisotropic surfaces. *Phys. D*, 112(3-4):381–411, 1998.

- [18] S. Torabi, J. Lowengrub, A. Voigt, and S. Wise. A new phase-field model for strongly anisotropic systems. *Proceedings of the Royal Society A: Mathematical, Physical and Engineering Science*, 465(2105):1337–1359, May 2009.
- [19] S. M. Wise, C. Wang, and J. S. Lowengrub. An energy-stable and convergent finite-difference scheme for the phase field crystal equation. *SIAM J. Numer. Anal.*, 47(3):2269–2288, 2009.
- [20] S. Wise, J. Kim, and J. Lowengrub. Solving the regularized, strongly anisotropic Cahn-Hilliard equation by an adaptive nonlinear multigrid method. *Journal of Computational Physics*, 226(1):414–446, September 2007.
- [21] X. Yang, J. J. Feng, C. Liu, and J. Shen. Numerical simulations of jet pinching-off and drop formation using an energetic variational phase-field method. *J. Comput. Phys.*, 218:417–428, 2006.
- [22] J. Zhu, L.-Q. Chen, J. Shen, and V. Tikare. Coarsening kinetics from a variable-mobility Cahn-Hilliard equation: Application of a semi-implicit fourier spectral method. *Physical Review E*, 60(4):3564, 1999.